

A Thin Cambered Bent Biomimetic Wind Turbine Blade Design by Adopting the 3D Wing Geometry of a Borneo Camphor Seed[#]

Yung-Jeh CHU^{1*}, Heung-Fai LAM^{1,2} and Hua-Yi PENG²

1 Department of Architecture and Civil Engineering, City University of Hong Kong, Tat Chee Avenue, Kowloon, Hong Kong
(Corresponding Author)

2 School of Civil and Environmental Engineering, Harbin Institute of Technology, Shenzhen, China

ABSTRACT

This study proposed a new thin cambered bent biomimetic wind turbine design that adopted the 3D geometry of the wing of a Borneo camphor seed sample. The wings of the Borneo camphor seed are thin, cambered, and bent. The unique geometry and orientation of the wings cause the seed to autorotate during propagation, subsequently slowing down its falling speed. It was presumed that by mimicking the wings of a Borneo camphor seed, a high-performance biomimetic wind turbine design could be proposed since the wind turbine, and Borneo camphor seed shares a similar rotating mechanism. Computational fluid dynamics was adopted to predict the power coefficient, thrust coefficient, and torque of the proposed biomimetic wind turbine models. The results show that the highest power coefficient was 0.3861 for the biomimetic wind turbine model, which is 20.14% higher than that of a benchmark case when the fold axis and fold angles are equal to 30° and 30°, respectively. The findings of this study concluded that the proposed biomimetic wind turbine design is cost-effective and worthy of further investigation.

Keywords: Wind turbine, biomimetics, CFD, Borneo camphor, 3D scanning, reverse engineering

NOMENCLATURE

<i>Abbreviations</i>	
CFD	Computational Fluid Dynamics
MRF	Moving Reference Frame
SIMPLE	Semi-Implicit Method for the Pressure-Linked Equations
STL	Stereolithography
TSR	Tip Speed Ratio
<i>Symbols</i>	
C_p	Power coefficient
$C_{p,Peak}$	Peak power coefficient

C_T	Thrust coefficient
E	Experimental result
F_T	Thrust
P	Blade root
r	Radial distance
R	Rotor radius
R_h	Hub radius
S	Simulation result
U	Wind speed
α_r	Fold axis angle
θ_r	Fold angle
ρ	Air density
τ	Torque
ω	Rotational speed

1. INTRODUCTION

The definition of biomimetics, according to Ref. [1], can be summarized as the study of biological structure, mechanism, and process to produce product likewise by mimicking. Biomimetics is a kind of reverse engineering where natural objects such as flora and fauna were mimicked in the design of new technology, which may enhance the performance of the product. This is based on the presumption that the natural world design is optimized while the human design is flawed. On top of that, it was known that there exist a lot of problems unsolvable due to the limitation of classical engineering theories; thus, these have become the motivation for implementing biomimetics into technologies. In the field of wind turbine technology, biomimetics has been utilized to invent new wind turbine designs.

There were some examples where biomimetics was successfully utilized in wind turbine blade designs. For example, according to Ref. [2], a bird wing-inspired small-scale wind turbine blade was proposed. This bird wing-inspired wind turbine, also called the flexion blade exhibits higher performance when compared to the conventional wind turbine design. Another example of

the biomimetic wind turbine can be referred to in Ref. [3], where the protuberance of humpback whale fins was mimicked in blade design. The experimental results show that the implementation of protuberance onto the leading edges of wind turbine blades improved its power performance. These examples highlighted the potential of biomimetics in improving the performance of wind turbine blade design.

The Borneo camphor (*Dryobalanops aromatica*) is a tropical tree that is native to Malaysia and Indonesia; that can reach a height of 65 m and produces winged seeds, according to Ref. [4]. The Borneo camphor has a history where it was desired by Arab traders in ancient times because of its usage as perfume and incense. The Borneo camphor seed generally consists of five wings surrounding a nut which the shape resembles a shuttlecock. Due to the conical shape of the Borneo camphor seed, it can align itself to face the oncoming relative wind during falling. The pitched wings interacting with the relative wind generate torque about the rotational axis of the seed and initiate autorotation. This autorotation expands the wings radially outward, which increases its rotor size, increases lift and drag forces, and subsequently slows down the descent of the winged seed. It is this flight mechanism that intrigues researchers about whether its geometry is suitable to be mimicked in the wind turbine blade design.

Previous studies of Borneo camphor seed-inspired wind and water turbines were conducted by researchers, as shown in Ref. [5–10]. These wind and water turbines were based on photos of a seed sample where the geometrical features such as chord, camber, and outlines of leading and trailing edges were extracted. However, these biomimetic wind and water turbine models were not representing the natural wing geometry of the Borneo camphor seed. Thus, 3D scanning technology was implemented in the current study to extract the natural shape of the wing of a Borneo camphor seed. Given the natural capability of the Borneo camphor seed in autorotation, it was presumed that its wings might have high performance acting as wind turbine blades. Thus, this study investigated the performances of a 3D scanned wing of the Borneo camphor seed as wind turbine blades.

2. BORNEO CAMPHOR SEED MODEL AND BLADE CONFIGURATIONS

A seed sample was acquired from the vicinity of a Borneo camphor tree located at the Department of Geology, Faculty of Science, University of Malaya. A photo of the mentioned location can be referred to Ref. [6]. The seed sample was then sent to a metrology company for 3D scanning. Fig. 1 shows the 3D-scanned

model of the mentioned Borneo camphor seed sample. An ATOS core scanner with a point spacing of 0.2 mm was used to scan the seed sample. The scanned geometry was saved in the stereolithography (STL) format and then imported into the ANSYS SpaceClaim software for further processing. After the cleaning process of the STL file of the seed, the sample was completed, and one of the wings was isolated and scaled up to fit a 0.2 m diameter hub and 1 m diameter rotor. The scaled-up wing is as shown in Fig. 2. It can be observed that the wing of the Borneo camphor seed is thin, cambered, and bent. Fig. 3 shows the cross-sections of the scaled-up wing model.



Fig. 1 3D-scanned model of the Borneo camphor seed sample.

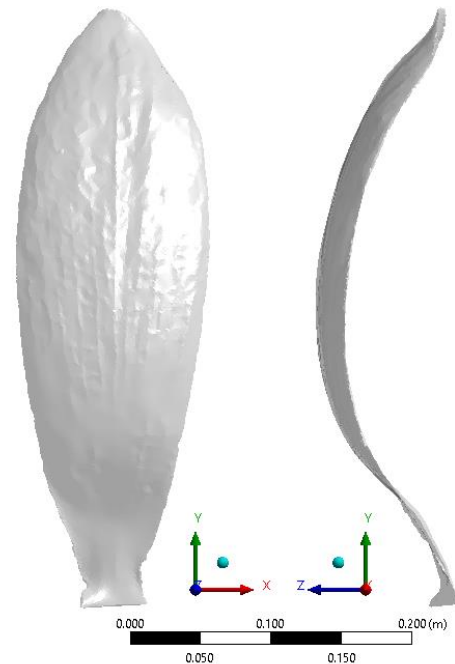


Fig. 2 Views of the convex surface (left) and side (right) of a scaled-up wing model.

All the wing sections are thin except those located near the hub, such as at $r/R=0.2$. The chord length was short at $r/R=0.2$, and then it increased radially outward until $r/R=0.65$ and then decreased until it reached the tip at $r/R=1$. The cambers of these wing sections were high. The wing was bent along its span, forming a curvature

among its root, mid-section, and tip. These unique geometrical features are different than that of the conventional wind turbine blade sections, which consist of teardrop shape airfoil sections such as the NACA airfoil series. Thus, it was expected that the performance of the biomimetic wind turbine would be different than that of the conventional wind turbine design. The thin cambered bent features also mean that cheaper blade fabrication methods such as plastic or metal sheet forming can be used. For example, vacuum forming with a plastic sheet can be used to fabricate the proposed biomimetic wind turbine blades.

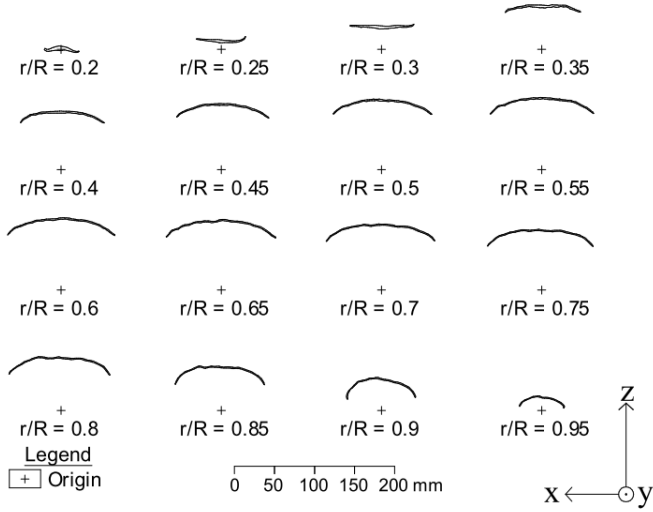


Fig. 3 Cross-sections of the scaled-up wing model. Where r means radial distance and R means radius.

The layout of the wing where the view is at the concave surface is shown in Fig. 4. All the related parameters were illustrated in the mentioned layout. P is the location of the blade root where the fold axis passes through, θ_r is the fold angle, α_r is the fold axis angle, R is rotor radius, R_h is the hub radius, and r is the radial distance measured from the origin.

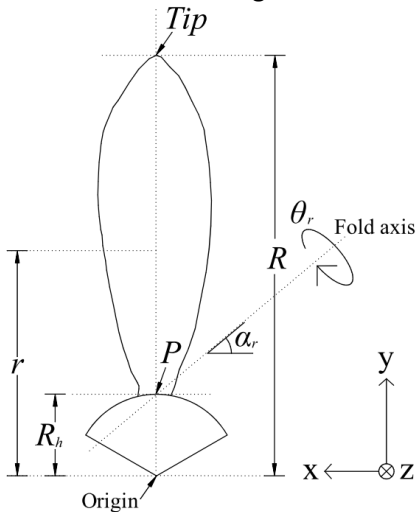


Fig. 4 Sketch showing the layout of the wing attached to the hub with its associated parameters.

The α_r and θ_r are the main parameters in concern that will alter the performances of the biomimetic wind turbine in terms of power coefficient, torque, and thrust coefficient. Thus, nine different configurations of the α_r and θ_r was designated as shown in Table 1. The range of α_r and θ_r were from 15° to 45° with 15° intervals. It must be noted that the rotor radius was 0.5 m before folding; in other words, when α_r and θ_r are both equal to zero. The rotor radii of the biomimetic wind turbine models were reduced after folding.

Table 1: Summary of various configurations of the biomimetic wind turbine models.

Case	Fold axis angle, α_r ($^\circ$)	Fold angle, θ_r ($^\circ$)	Rotor radius, R (m)
1	15	15	0.4873
2	30	15	0.4898
3	45	15	0.4932
4	15	30	0.4502
5	30	30	0.4604
6	45	30	0.4740
7	15	45	0.3918
8	30	45	0.4152
9	45	45	0.4453

3. COMPUTATIONAL FLUID DYNAMICS (CFD) MODELLING

ANSYS Fluent was used to model the airflow surrounding the rotating biomimetic wind turbine. A steady-state solver, namely the multiple reference frame (MRF), was adopted as the CFD simulation model. The semi-implicit method for the pressure-linked equations (SIMPLE) algorithm was chosen as the numerical procedure for solving the fluid flow equations. The SST k - ω model was selected as it was one of the best turbulence models available for wind turbine simulation. A second-order spatial discretization scheme was chosen. To reduce computational time, only one-third of the wind turbine was modeled, as shown in Fig. 5. The CFD domain was divided into two, namely the stator and rotor domains. The stator domain consists of wall boundary at the arc surface of the circular sector and periodic wall boundaries at the radii surfaces. The rotor domain is where the wind turbine blade and hub are located. An interface boundary was located in between the boundaries of the stator and rotor domain, separating the two domains. The dimension of the whole domain was similar to Ref. [10].

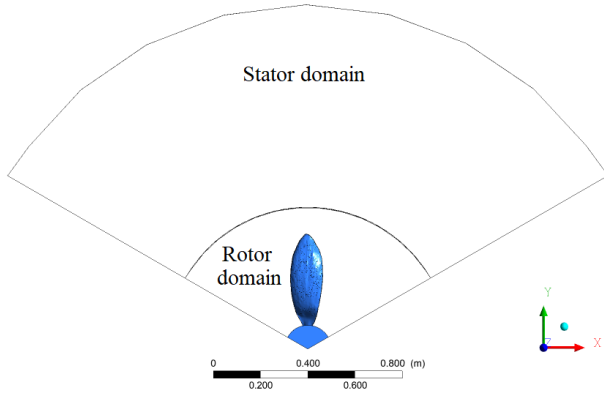


Fig. 5 Section view of CFD model domain showing the wing, hub, stator, and rotor.

The boundary conditions include 10 m/s wind speed, 0.35% of turbulence intensity, 1.225 kg/m^3 of air density, and $1.46 \times 10^{-5} \text{ m}^2/\text{s}$ of kinematic viscosity. A benchmark wind turbine model from Ref. [11] was adopted for the purpose of validation and performance comparison. The geometry of the benchmark wind turbine in this study is similar to the one modeled in Ref. [10], where the rotor diameter is 1 m, the SD8000 airfoil was adopted as the blade section throughout the span, and the pitch angle was zero degrees. There was no twisting on the blade sections along the span of the benchmark wind turbine model. The prism cell type was used on all the wind turbine blade surfaces, while the polygonal cell type was used for the rest of the meshes in the rotor and stator domains. The reason for adopting polygonal meshes is that it was known to enhance convergence and reduce computational time. The mesh layout of the biomimetic wing section at $r = 0.43 \text{ m}$ is as shown in Fig. 6.

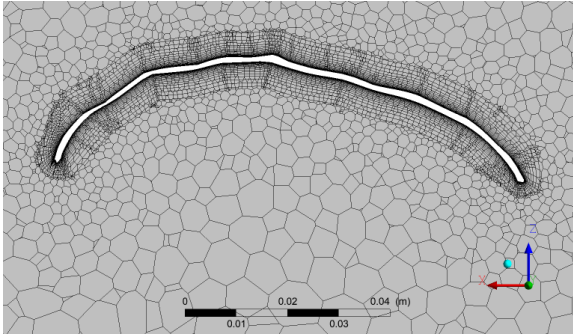


Fig. 6 Mesh layout of the wing section at $r = 0.43 \text{ m}$.

A mesh dependency test was done to verify that the mesh is adequate to produce accurate CFD results. It was tested that the fluid flow solution converged and almost matched the experimental results when the mesh sizes for turbine blade, rotor domain, and stator domain were 0.001 m, 0.07 m, and 0.36 m, respectively. Therefore, the same mesh properties were adopted from the validated benchmark wind turbine case and implemented into the

biomimetic wind turbine cases. It was presumed that the CFD results of the biomimetic wind turbine cases are as accurate as those of the benchmark wind turbine cases since they share the same mesh properties, boundary conditions, rotation speeds, and CFD domains. Further validations of the biomimetic wind turbine case results will be conducted in future studies when the wind tunnel facilities are available.

4. RESULTS AND DISCUSSIONS

The power coefficients, thrust coefficients, and torque of the proposed biomimetic wind turbine were analyzed. The equations for tip speed ratio, power coefficient, and thrust coefficients from Ref. [12] are as follow:

$$TSR = \frac{\omega R}{U} \quad (1)$$

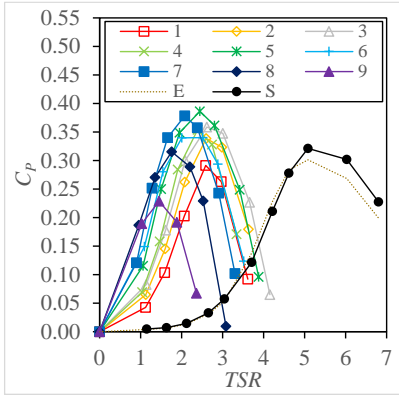
$$C_p = \frac{\omega \tau}{0.5 \rho \pi R^2 U^3} \quad (2)$$

$$C_T = \frac{F_T}{0.5 \rho \pi R^2 U^2} \quad (3)$$

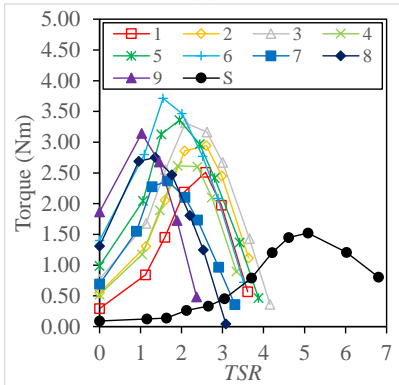
where ω is the rotational speed in rad/s, R is the radius of the rotor in m, U is the wind speed in m/s, τ is the torque in N, ρ is air density in kg/m^3 , and F_T is thrust in N.

All the C_p Versus TSR curves of the biomimetic wind turbine cases were shaped like an inverted “U” as shown in Fig. 7(a). This means that the maximum value of C_p can be deduced from each configuration. Since C_p is the most important quantity that will determine the efficiency of a wind turbine; the $C_{p,Peak}$ for each case was listed in Table 2 together with other less important quantities such as the starting torque and C_T at $C_{p,Peak}$. It can be observed that the magnitude of C_p versus TSR curves varies according to different configurations of α_r and θ_r values. The highest $C_{p,Peak}$ value was 0.3861 from case number five of the biomimetic wind turbine model when the α_r and θ_r are equal to 30° and 30° respectively. The mentioned $C_{p,Peak}$ value is 20.14% higher than that of the benchmark case, which means that the proposed biomimetic wind turbine model outperformed the benchmark wind turbine model in terms of power efficiency at certain fold axis and fold angles configurations. The torque versus TSR curve also exhibits the inverted “U” shape, as shown in Fig. 7(b). The maximum torque is not of concern in this study as this quantity does not contribute to the power performance. The power is equal to torque multiplied by rotational speed, which means the maximum torque value may not pair with the optimized TSR value to form the $C_{p,Peak}$. However, the starting torque (torque at $TSR = 0$) is important as it affects the self-start capability of a wind turbine. A high starting torque means that the wind

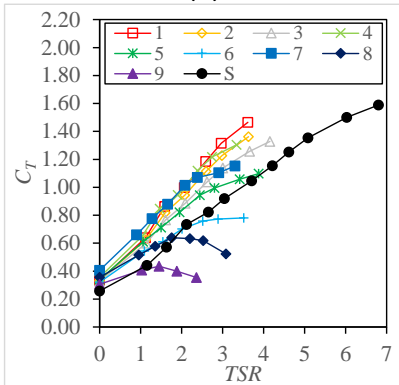
turbine will be able to overcome friction torque easily. The CFD results show that the starting torques of the proposed biomimetic wind turbine models are all higher than that of the benchmark case, indicating that the biomimetic wind turbines have better self-start capability. The C_T value increases as the TSR increase, as shown in Fig. 7(c). Some of the C_T versus TSR curves exhibit near-linear trends, while most of them are non-linear. This shows that when the α_r and θ_r are at low values, the biomimetic wind turbine generates more thrust forces than that when they are at high values. For example, case 1 has the highest C_T value while case 9 has the lowest.



(a)



(b)



(c)

Fig. 7 CFD results plotted as (a) C_p versus TSR , (b) torque versus TSR , and (c) C_T versus TSR graphs of biomimetic wind turbine cases. E is experimental data from Ref. [11], while S is simulation results of the benchmark case.

The C_T at $C_{p,peak}$ is just a quantity that takes into account the rotor thrust when the wind turbine operates at $C_{p,peak}$. The lower the C_T at $C_{p,peak}$ means the lower will be the thrust force acting on the wind turbine rotor. The C_T at $C_{p,peak}$ for all biomimetic wind turbine cases is lower than that of the benchmark case. This means that the supporting structure of the proposed biomimetic wind turbine is expected to be cheaper than that of the benchmark case if they were to be implemented in real-world applications. It can be observed that the range of $TSRs$ for the biomimetic wind turbine cases is lower than that of the benchmark wind turbine case. This means that the proposed biomimetic wind turbine is suitable to operate at low rotational speeds. The advantage of operating at low rotational speed is the low noise generated at the blade tip, which will reduce its impact on its surrounding environment.

Table 2: Summary of $C_{p,peak}$, starting torque, and C_T at $C_{p,peak}$ for all wind turbine cases.

Case	$C_{p,Peak}$	Starting Torque (Nm)	C_T at $C_{p,Peak}$
1	0.2914	0.2945	1.1844
2	0.3384	0.5477	1.1146
3	0.3586	0.7694	1.0390
4	0.3538	0.5200	1.1182
5	0.3861	0.9889	0.9434
6	0.3403	1.4024	0.7583
7	0.3781	0.6898	1.0140
8	0.3153	1.3106	0.6397
9	0.2288	1.8671	0.4346
Benchmark (CFD case)	0.3214	0.0901	1.3533

5. CONCLUSION

The main findings of this study can be summarized as the following:

1. The thin cambered bent features of the proposed biomimetic wind turbine indicate that the plastic or metal sheet forming fabrication method can be utilized in blade manufacturing. For example, vacuum forming with plastic sheet material can be used to fabricate the proposed biomimetic wind turbine blades. This lowers the cost of fabrication.
2. The highest $C_{p,peak}$ value was 0.3861 for the biomimetic wind turbine model, which is 20.14% higher than that of the benchmark case when the α_r and θ_r are equal to 30° and 30° , respectively. This indicates that the proposed biomimetic wind turbine model outperformed

the benchmark wind turbine model in terms of power efficiency at certain fold axis and fold angle configurations.

3. All biomimetic wind turbine cases exhibit higher starting torques when compared with the benchmark case. This means that the proposed biomimetic wind turbine design will have better self-start capability.
4. The C_T at $C_{P,Peak}$ for all biomimetic wind turbine cases is lower than that of the benchmark case. This low C_T at $C_{P,Peak}$ means a cheaper supporting structure is needed to be implemented onto the biomimetic wind turbines.
5. The low tip speed ratios operation made the proposed biomimetic wind turbine less noisy compared with the benchmark wind turbine design, which means it will have less impact on its surrounding during service.

Based on the abovementioned findings, it can be concluded that the proposed thin cambered bent biomimetic wind turbine blade design has the potential to outperform conventional wind turbine design. Therefore, the proposed biomimetic wind turbine blade design warrants further investigations, such as geometrical optimization to maximize its power output and geometrical simplification to reduce its fabrication cost.

ACKNOWLEDGEMENT

The work described in this paper was fully supported by a grant from the Research Grants Council of the Hong Kong Special Administrative Region, China [Project No. 9042509 (CityU 11210517)]. The authors also thank the First Metrology Sdn Bhd Malaysia for the 3D scanning service of the Borneo camphor seed sample.

REFERENCE

- [1] Bhushan B. Biomimetics: Lessons from Nature - an overview. *Philos Trans R Soc A Math Phys Eng Sci* 2009;367:1445–86.
- [2] Ikeda T, Tanaka H, Yoshimura R, Noda R, Fujii T, Liu H. A robust biomimetic blade design for micro wind turbines. *Renew Energy* 2018;125:155–65.
- [3] Huang GY, Shiah YC, Bai CJ, Chong WT. Experimental study of the protuberance effect on the blade performance of a small horizontal axis wind turbine. *J Wind Eng Ind Aerodyn* 2015.
- [4] Soepadmo E, Saw LG, Chung RCK. *Tree Flora of Sabah and Sarawak (Vol. 4)*. Kuala Lumpur: National Library of Malaysia; 2004.
- [5] Chu YJ. A new biomimicry marine current turbine: Study of hydrodynamic performance and wake using software OpenFOAM. *J Hydrodyn*

2016;28:125–41.

- [6] Chu YJ, Chong WT. A biomimetic wind turbine inspired by *Dryobalanops aromatica* seed: Numerical prediction of rigid rotor blade performance with OpenFOAM®. *Comput Fluids* 2017;159:295–315.
- [7] Chu YJ, Chong WT. Numerical study of conventional and biomimetic marine current turbines in tandem by using OpenFOAM®. *J Mech* 2018;34:679–93.
- [8] Chu YJ. *Conceptual Design and Performance Analysis of a Biomimetic Wind Turbine Inspired by the Dryobalanops Aromatica Seed*. Master Dissertation, University of Malaya, 2018.
- [9] Chu YJ, Lam HF. Comparative study of the performances of a bio-inspired flexible-bladed wind turbine and a rigid-bladed wind turbine in centimeter-scale. *Energy* 2020;213:118835.
- [10] Chu YJ, Lam HF, Peng HY. Numerical investigation of the power and self-start performance of a folding-blade horizontal axis wind turbine with a downwind configuration. *Int J Green Energy* 2021.
- [11] Lee MH, Shiah YC, Bai CJ. Experiments and numerical simulations of the rotor-blade performance for a small-scale horizontal axis wind turbine. *J Wind Eng Ind Aerodyn* 2016;149:17–29.
- [12] Manwell JF, McGowan JG, Rogers AL. *Wind Energy Explained: Theory, Design and Application*. 3rd ed. West Sussex, United Kingdom: John Wiley & Sons; 2010.